Fayoum University Faculty of Engineering, 2024, Vol: 7(2), 256-263
https://fuje.journals.ekb.eg/
ISSN Online: 2537-0634
ISSN Print: 2537-0626

Sensitivity of a Micro-scale Pump Flow Rate to Actuation Frequency Change

Gamal R. H. Abo Elyamin[1,*], Khalid H. M. Abdalrahman[1]

[1]Mechanical Power and Energy Engineering Department, Faculty of Engineering, Minia University, Minia 61519, Egypt

*Corresponding author: Gamal R. H. Abo Elyamin (gamalrabeh@mu.edu.eg).

How to cite this paper: Abo Elyamin, G.R.H. & Abdalrahman, K.H.M. (2024). Sensitivity of a Micro-scale Pump Flow Rate to Actuation Frequency Change. *Journal of Fayoum University Faculty of Engineering, Selected papers from the Third International Conference on Advanced Engineering Technologies for Sustainable Development ICAETSD, held on 21-22 November 2023, 7(2), 256*-263.
https://dx.doi.org/10.21608/fuje.2024.344039

Abstract

A three-dimensional computational fluid dynamics simulation for a micro-scale pump has been performed to investigate the sensitivity of the flow rate to frequency change during pump and supply phases. Applying dynamic mesh under different diaphragm actuation frequencies (*8, 50, 100, 200, and 500 Hz*) and sinusoidal oscillation amplitude of *6.0 μm* the results showed that at frequency $f \geq 100$ *Hz* the flow separation has been formed in the diffuser direction for both supply and pump phases. At low frequency $f \leq 50$ *Hz* there is no flow separation in the diffuser or the nozzle direction. The large recirculation zone is created at the diffuser bottom wall side. The flow separation was found to be frequency and direction dependent for the micro-diffuser half angle of *5o*. The net flow rate increased linearly with the frequency while the net flow per cycle was less sensitive to the change of the frequency.

Keywords

Micro-scale pump, Microelectronic cooling, CFD simulation, Frequency sensitivity

1. Introduction

A micro-scale pump is a pump system in micro-scale dimensions which is used in many applications such as biochemistry (Andersson et al., 2001), medicine (Cui et al., 2008 & Dereshgi, 2018 & Armita et al., 2022), biomedical (Gharib et al., 2023), flow separation control (Lim et al., 2005), and microelectronic cooling (Ma et al., 2008 & Verma et al., 2009). To improve the cooling process in microelectronic equipment the coolant must be forced through the micro heat exchanger or microchannels by integrating a tiny, low cost and reliable pump (Singhal et al., 2005). According to micro-scale pump classification (Laser et al., 2004) the valve-less micro-scale pump is a displacement micropump which can be actuated in several ways such as; pneumatic, thermo pneumatic, piezoelectric, electrostatic, bimetallic, and shape memory effect and electromagnetic (Yi-Fang et al., 2020). The designs of micro-scale pumps are challenging in terms of model complexity and limited knowledge of device physics on the micro-scale. Therefore, modelling strategies for micro-scale pumps have involved CFD simulation to pre-check the model design and avoid design problems (Wang et al., 2006). Some research efforts have been performed to model the valve-less micropump by different ways, for instance, lumped mass model (Olsson et al., 1999), electrical equivalent networks (Tarik et al., 1996), analytical analysis (Li et al., 2003), and numerical

or computational simulation (Hwang et al., 2008, Olsson et al., 2000, Yao et al., 2007, Zhang et al., 2005). The oscillation frequency effect on valve-less micropump flow rate has not been investigated in (Olsson et al., 2000) but the three-dimensional model was recommended to cope with the problems of low Reynolds number. However, a two-dimensional model has been employed (Zhang et al., 2005). (Yao et al., 2007) used symmetric geometry to reduce the problem size while this choice is not a good approximation for diffusers because the diffusers might have unsteady flow (Olsson et al., 2000). From the available literature, there is a lack of knowledge about flow rate sensitivity according to frequency change during a complete working cycle in a micro-scale pump. A complete working cycle of a valveless micro-scale pump consists mainly of the pump phase and supply phase. In the supply phase shown in Figure 1. (a), the diaphragm moves upward the pump chamber volume increases then the pressure decreases as a result the fluid flows into the pump chamber through the inlet and outlet diffuser/nozzle elements in such a way more flow passes through the inlet diffuser/nozzle element because it acts as a diffuser while the outlet diffuser/nozzle element acts as a nozzle. In the pump phase shown in Figure 1. (b), the diaphragm moves downward and the pump chamber volume decreases then the pressure increases so the fluid flows out from the pump chamber through the inlet and outlet diffuser/nozzle elements. In this case, the inlet diffuser/nozzle element acts as a nozzle while the outlet diffuser/nozzle element acts as a diffuser. Pressure recovery in the diffuser direction is higher than pressure recovery in the nozzle direction, and for a given pressure difference the element passes more fluid in the diffuser direction than in the nozzle direction (Gravesen et al., 1993). Hence, during a complete actuation cycle of the diaphragm over a time period which produces supply and pump phases net flow from the inlet to the outlet is generated resulting from the difference of flow rates through the inlet and outlet diffuser/nozzle elements.

In the current work, a 3-D CFD simulation has been performed using the Fluent solver to solve the flow and calculate the flow rate generated under sinusoidal oscillation amplitude of 6.0 μm and different actuation frequencies of 8 Hz, 50 Hz, 100 Hz, 200 Hz and 500 Hz.

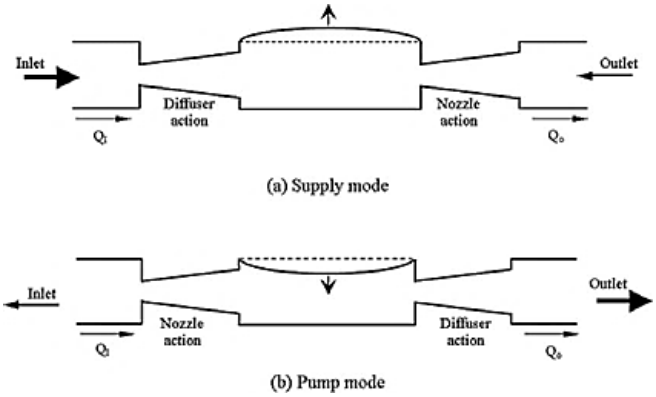

Figure 1. Pump principle of piezoelectric valveless micropump

2. Model geometry

The model used in this study is based on the dimensions in (Yao et al., 2007) and consists mainly of the pump chamber, diffuser/nozzle valves, diaphragm, and the actuator besides the linking parts between the pump chamber and diffuser/nozzle elements. The isometric view is shown in Figure 2 and the geometric dimensions of the micropump model are illustrated in **Table 1**.

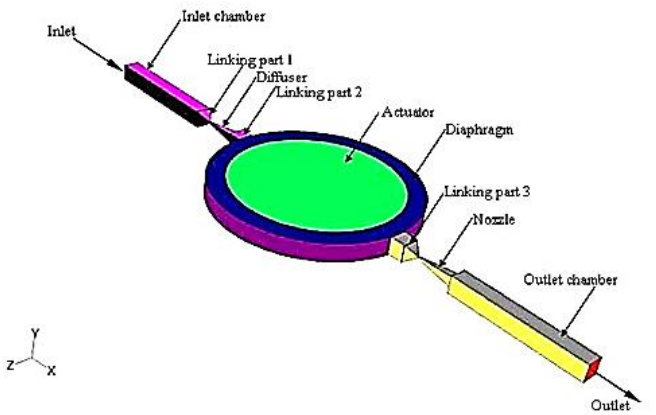

Figure 2. Isometric view of the micropump model (Yao et al., 2007)

Table 1- Geometric dimensions of the micropump model

Micropump part	Dimension (mm)
In/out chamber length	3.95
In/out chamber width	0.5
Diffuser/nozzle length	1.25
Diffuser/nozzle throat width	0.04
Diffuser/nozzle wide port width	0.3
Diffuser/nozzle half angle	5°
Pump chamber diameter	6
Base groove diameter	5
Base groove height	0.1
PZT layer diameter	5
Total Micropump length	18
Total Micropump height	0.55
Total Micropump width	6

3. Theoretical analysis

3.1. Total pressure loss coefficient

The total pressure loss coefficient ξ for flow through a gradually expanding diffuser, gradually contracting nozzle, or a sudden expansion or contraction in an internal flow system is defined as the ratio of pressure drop ΔP across the device to the velocity head upstream of the device (Singhal et al., 2004, Stemme & Stemme, 1993, Wu, 2003). The pressure drop in the direction of the flow is the decrease in pressure from one point to another through the internal flow system.

$$\xi = \Delta P / 0.5 \rho\, v^2 \quad (1)$$

Where ΔP is the pressure drop (N/m^2), ρ is the fluid density (kg/m^3), and v is the fluid velocity (m/s).

3.2. Diffuser efficiency

The diffuser efficiency η of a diffuser/nozzle element is defined as the ratio of the total pressure loss coefficient for flow in the nozzle direction ξ_n to that for the flow in the diffuser direction ξ_d

$$\eta = \xi_n / \xi_d \quad (2)$$

From Equation (2) the flow direction will depend on the diffuser efficiency so, if $\eta > 1$ the flow will be in the diffuser direction, while $\eta < 1$ will lead to pump of the fluid in the nozzle direction.

If $\eta = 1$ this means equal pressure drop in both the nozzle and diffuser directions, leading to no flow rectification.

3.3. Flow rectification efficiency

The flow rectification efficiency of a valveless micropump χ is the ability of the valveless micropump to direct the flow in one specific direction. It can be expressed as:

$$x = (Q_+ - Q_-)/(Q_+ + Q_-) \quad (3)$$

Where Q_+ is the flow rate in the forward and Q_- is the flow rate in the backward directions. The higher χ corresponds to better flow rectification.

3.4. Flow governing equations

Equations of motion for 3-D, incompressible, viscous, unsteady state flow in Cartesian (x-y-z) co-ordinates have been used as explained in (Versteeg & Malalasekera, 1995) to simulate the laminar flow inside the valveless micropump.

- Continuity

$$\partial\rho/\partial t + \nabla.(\rho U) = 0 \quad (4)$$

- Navier-Stokes equations in laminar form

In x-direction:

$$\boldsymbol{\partial(\rho u)/\partial t + \nabla.(\rho u U) = -\partial P/\partial x + \nabla.(\mu \nabla u)} \quad (5.a)$$

In y-direction:

$$\partial(\rho v)/\partial t + \nabla.(\rho v U) = -\partial P/\partial y + \nabla.(\mu \nabla v) \quad (5.b)$$

In z-direction:

$$\partial(\rho w)/\partial t + \nabla.(\rho w U) = -\partial P/\partial z + \nabla.(\mu \nabla w) \quad (5.c)$$

Where P, ρ, μ, ∇, u, v, w and U are pressure, fluid density, dynamic viscosity, standard spatial grad operator, velocity component in x-direction, velocity component in y-direction, velocity component in z-direction and velocity vector ($u_i + v_j + w_k$), respectively.

4. CFD Simulation

4.1. Diaphragm deflection

The source of actuation of the fluid inside the pump chamber is the piezoelectric actuator which consists of

the piezoelectric disc attached to the elastic membrane. When sinusoidal alternate voltage $[V = V_o \sin(2ft)]$ is applied to the piezoelectric layer the membrane will expand or contract, and then the pump chamber volume and pressure are changed over an interval of time as a result fluid flow will be generated through the whole micropump by the function of diffuser/nozzle elements. A user-defined function *(UDF)* has been used to control the deflection of the oscillating membrane according to the deflection amplitude *A* and frequency *f*. The deflection amplitude is the most important parameter for the simulation so the maximum center deflection of the diaphragm according to the voltage applied has been taken from (Zhang & Wang, 2006) as shown in **Figure 3**. The diaphragm was assumed to move in a sinusoidal fashion and simulated by:

$$\boldsymbol{y(r,t) = A\cos\left(\frac{\pi r}{D}\right)\sin(2\pi f t)} \quad (6)$$

Where *y* is the maximum diaphragm deflection, *r* is the radial distance, *t* is the flow time and *D* is the actuator diameter.

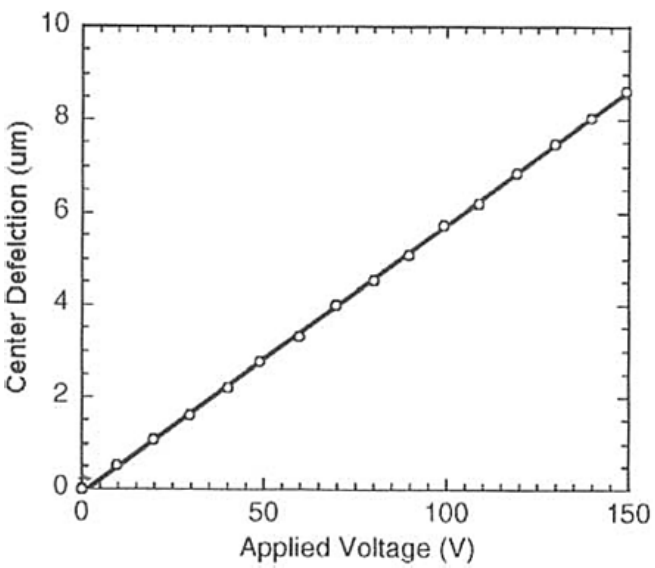

Figure 3. Diaphragm deflection under different applied voltage (Zhang et al., 2006)

4.2. Geometry and grid generation

GAMBIT as an operator interface has been used to create the 3-D geometry and then generate the mesh for the model that is used to solve the flow. The geometry has been created by using the "bottom-up" approach. The unstructured mesh has been generated by using the tetrahedral/hybrid elements and TGrid type scheme. The mesh for the typical model consists of (76019) total number of grid nodes and (351442) total number of elements or cells.

4.3. Boundary conditions

The inlet and the outlet boundary condition have been set to be inlet-vent and outlet-vent, respectively because both of the inlet and outlet ports in the micropump work as inlet during the supply phase and outlet during the pump phase according to the diaphragm oscillation. The flow is assumed to be unsteady, viscous, and laminar with no-slip conditions near the wall. All the walls of the micropump are assumed to be fixed except for the diaphragm, which is an oscillating diaphragm and the oscillation of this diaphragm is governed by a compiled user defined-function to simulate the diaphragm oscillation using dynamic mesh.

4.4. Time step settings

Time step size Δt is the key for the solution accuracy in unsteady flow problems. Hence, the value of time step size Δt is changed according to the change in frequency and number of time steps N by applying the relation (Yao et al., 2007):

$$\Delta t = 1/(f \times N) \quad (7)$$

According to Equation (7) the value of the proper time step size at a certain frequency value was calculated at constant *N* = 400 and different frequency values *f*.

4.5. Mesh sensitivity

Grid independence studies were performed to minimize the computational effort. Three different meshes with different numbers of elements mesh 1 of (56845 elements), mesh 2 of (351442 elements), and mesh 3 of (918439 elements) have been examined for grid independence. The flow rate is plotted as a function of time at zero back pressure. **Figure 4** illustrates the outlet flow rate for the three different meshes at a frequency of 50Hz and amplitude of 70 μm. From **Figure 4** it is obvi-

ous that there is some difference in the flow rates resulting from the three different meshes. The coarse mesh (mesh 1) has not been used to avoid the deviation of the flow rate at a steady state from the mesh independence. Mesh 3 is very fine and needs high computational effort without any significant improvement of the net flow rate so that mesh 2 of (351442 elements) has been selected to simulate the unsteady flow in the valve-less micropump.

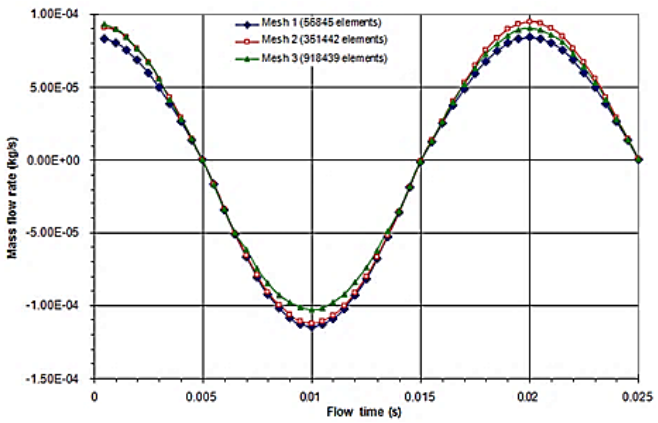

Figure 4. Grid independence for flow rate at outlet for 50 Hz and 70 µm

4.6. Validation

The flow visualization from the experimental work in (Chen-li & Zone, 2007) has been compared with the current CFD simulation using Fluent solver. A combined structure and unstructured mesh of 53173 elements has been used to perform the simulation. The inlet boundary condition was set to be a pressure inlet of 550 pa gauge pressure, the outlet boundary condition was set to be a pressure outlet of 0 pa gauge pressure and the Reynolds number was 20.2. The streamtraces resulted from the CFD work compared with the experimental flow visualization and showed a reasonable agreement as shown in **Figure 5**.

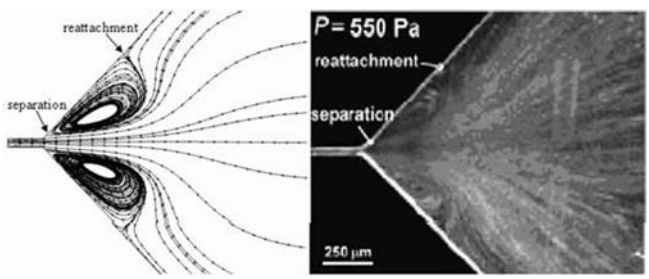

Figure 5. Diffuser flow separation comparison for validation

The rectification efficiency (χ) has been taken as a performance indicator. The rectification efficiency of diffuser-nozzle micropumps reported in the literature is generally between 1% and 20% (Singhal et al., 2004) and the rectification efficiencies for these models range from 2.75% to 13.1%, which are consistent with the reported range.

5. Results and discussion

Inlet and outlet flow rates at 500 Hz frequency and 6µm amplitude are illustrated in **Figure 6** the complete cycle consists of the pump phase and the supply phase so the velocity vectors and stream traces are depicted for the two phases at a frequency of 500 Hz.

5.1. Pump phase

In this phase, the maximum deflection was achieved downward and the flow was subjected to maximum pump force. The maximum velocity occurred in the outlet diffuser. The maximum velocity magnitude at the inlet diffuser throat during the pump phase was less than the velocity magnitude at the outlet diffuser throat which means more flow produced in the outlet port according to the mass conservation law. Stream traces are used to illustrate the flow separation in the valve-less micropump as an internal flow system. During the pump phase at the 500 Hz case, no recirculation zones or flow separations were formed in the inlet diffuser and the flow was attached to the side walls as shown in **Figure 9**. In contrast, a big recirculation zone covering about 85 percent of the length of the diffuser bottom wall occurred in the outlet diffuser. Two main recirculation regions and two secondary recirculation zones were formed in the pump chamber the first main one was located at 0.00675 m of the pump length near the inlet diffuser exit its rotation direction was clockwise opposite to the flow direction from the pump chamber to the inlet diffuser.

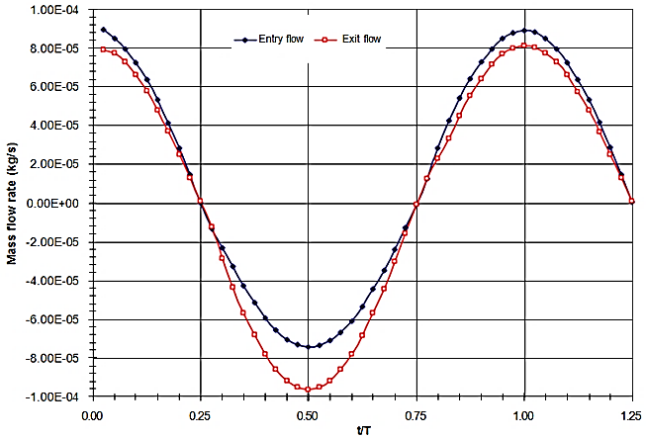

Figure 6. Inlet and outlet flow rates at 500 Hz and 6 µm

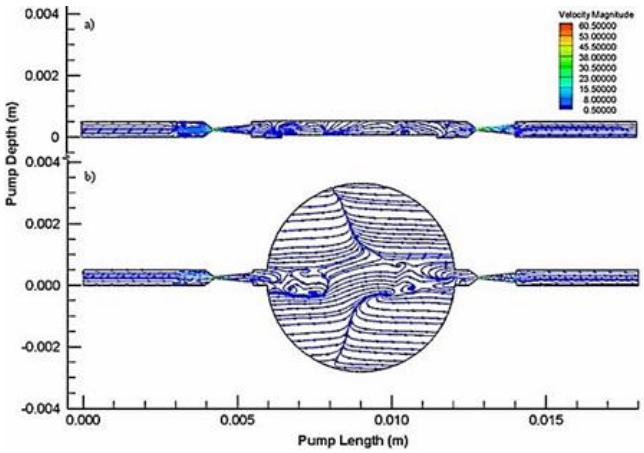

Figure 7. Streamtraces during pump phase for 500 Hz-6 µm case at;
a) vertical section b) horizontal section

The second main recirculation zone was located near the outlet diffuser entrance at 0.0105 m of the pump length its rotation direction was counterclockwise opposite to the flow direction from the pump chamber to the outlet diffuser as shown in **Figure 7**. The size of the first main recirculation zone was larger than the size of the second main one which means that the first one blocked a larger volume in the flow path towards the inlet diffuser. Two small recirculation zones were created in the outlet chamber due to the sudden expansion and another two recirculation zones of larger size were formed in the inlet chamber immediately after the diffuser throat due to gradual expansion. The flow rectification was not affected only by the recirculation regions in the outlet diffuser but also by the recirculation regions in the whole micropump.

5.2. Supply phase

The maximum velocity magnitude achieved in the inlet diffuser throat. During the supply phase, the flow came into the pump chamber from the diffuser/nozzle elements as the pressure outside the pump chamber was higher than the pressure inside the pump chamber because the maximum deflection occurred upward and the flow was subjected to the minimum pump force. The maximum velocity magnitude at the outlet diffuser throat was less than that at the inlet diffuser throat then more flow passed from the inlet diffuser to the pump chamber. From **Figure 9** during the supply phase at the 500 Hz case, the recirculation zones were created in the inlet diffuser. The big recirculation zone and flow separation generated at the diffuser bottom wall covered about 84 percent of the length of the diffuser bottom wall. The two small recirculation zones generated at the top wall covered about 42 percent of the length of the diffuser wall. In contrast, there was no recirculation zone occurred at the outlet diffuser. From **Figure 8** the two main recirculation zones that were observed in the pump phase shrank due to the change of the working phase from pump to supply and another two recirculation regions were formed closer to the inlet and outlet diffusers. The location at 0.00575 m of the pump length had two recirculation zones the lower one was bigger than the upper one. The rotation direction of the lower one was clockwise against the rotation direction of the upper one. The combination of these two recirculation zones supported the flow direction from the inlet chamber to the pump chamber. At 0.01175 m of the pump length two recirculation regions were observed, the lower one was bigger in size and the rotation direction was counter-clockwise opposite to the upper one. The existence of these recirculation zones and the function of the diffuser affected the flow rectification and pump performance by means of getting more flow inside the pump chamber from the inlet diffuser.

For the full range of frequency from 8 Hz to 500 Hz, there were no recirculation zones or flow separation in the diffuser/nozzle elements at low frequency f ≤ 50Hz. The onset of the flow separation started at f ≥ 100 Hz. While the recirculation regions for 100 Hz were observed in the outlet diffuser during the pump phase and in the inlet diffuser during the supply phase, no recirculation regions were observed in the nozzle direction (converging direction) during the pump or supply phase. Further increase in the excitation frequency leads to an increment of the recirculation zone size and secondary recirculation zone formation in the inlet diffuser during the pump phase as shown in **Figure 9**.

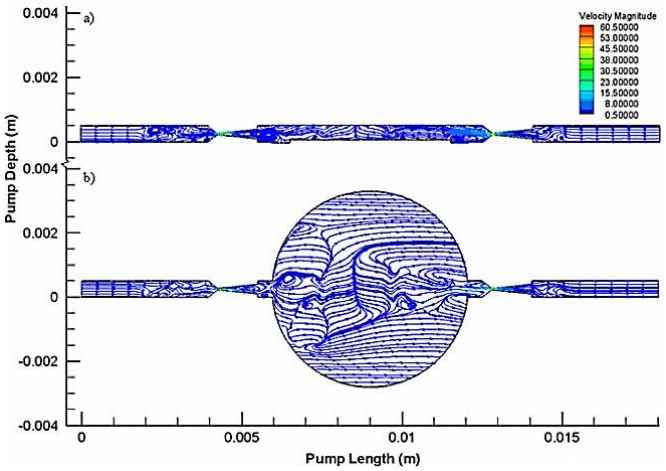

Figure 8. Streamtraces during supply phase for 500 Hz-6 µm case at; a) vertical section b) horizontal section

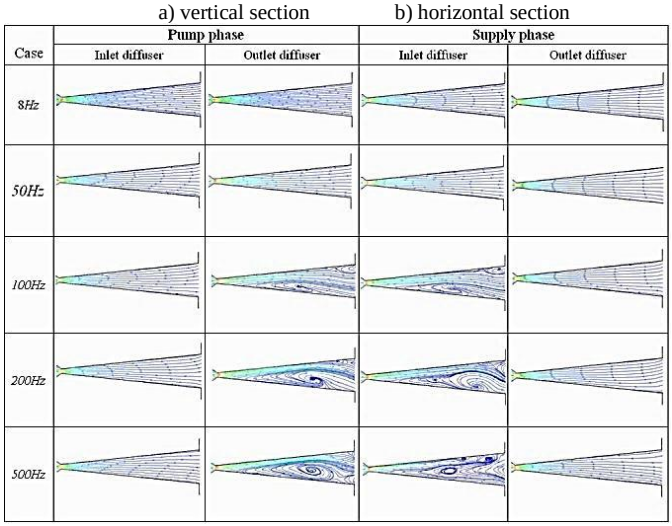

Figure 9. Recirculation zones and flow separation for pump and supply phases

For a complete cycle, the net mass flow rate and net mass flow per cycle are illustrated in **Figure 10** for different frequencies. The net mass flow rate increased linearly with the frequency from 8 Hz to 500 Hz at amplitude of 6 µm because the inertial effect of the transferred fluid is neglected. The highest net mass flow rate of 1.96 µL/min was generated at a frequency value of 500 Hz. The net mass flow per cycle has no significant change due to the frequency increasing.

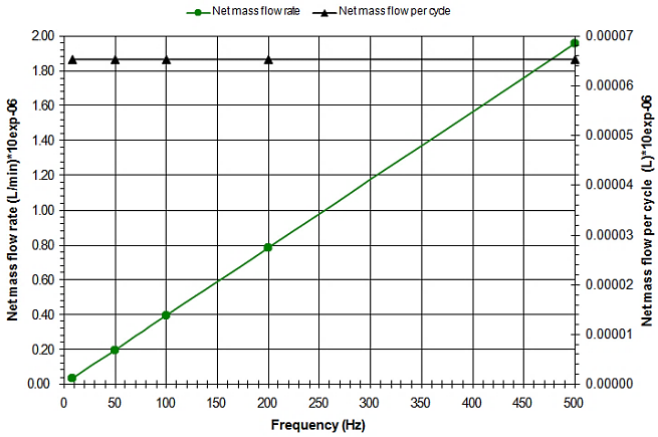

Figure 10. Net mass flow rate and net mass flow per cycle for different frequencies

6. Conclusions

A 3-D CFD flow simulation has been performed to investigate the sensitivity of the flow rate to frequency change during pump and supply phases in a micro-scale pump. The net mass flow rate increased linearly with frequency and the maximum generated flow rate at a frequency of 500 Hz and amplitude of 6 µm was 1.96 µL/min. The net mass flow rate per cycle was less sensitive to the frequency change. No flow separation occurred in the nozzle direction (converging direction) for flow under the full range of frequency 8–500 Hz. In contrast, the flow separation occurred in the diffuser directions for both pump and supply phases at $f \geq 100$ *Hz*.

References

Andersson, H., Van der Wijngaart, W., Nilsson, P., Enoksson, P., & Stemme G. (2001). A valve- less diffuser micropump for microfluidic analytical systems. Sensors and Actuators, B 72:259-265.

Armita, N., Mohammad, S., & Siamak, H. (2022). Design of the micropump and mass-transfer compartment of a microfluidic system for regular nonenzymatic glucose measurement. Biotechnology Reports, vol. 34, pp. e00723.

Chen-li, S., & Zone, Y. (2007). Effects of the half angle on the flow rectification of a microdiffuser. Journal of Micromechanics and Microengineering 17:2031-2038,

Cui, Q., Liu, C., & Zha, F. (2008). Simulation and optimization of a piezoelectric micropump for medical applications. International Journal of Advanced Manufacturing Technology 36:516-524.

Dereshgi, A., & Yildiz, Z. (2018). Investigation of electro-mechanical factors effecting piezoelectric actuator for valveless micropump characteristics. Journal of Engineering Science and Technology, vol. 13, no. 9, pp. 2843-2856.

Gravesen, P., Branebjerg, J., & Jensen, O. (1993). Microfluidics -

A review. Journal of Micromechanics and Microengineering 3:168-182.

Gharib, G., Bütün, I., Muganli, Z., Kozalak, G., Namli, I., Sarraf, S., Ahmadi, E., Toyran, E., Van Wijnen, J., & Koşar, A. (2023). Biomedical Applications of Microfluidic Devices: A Review. Biosensors, vol. 12, no. 11 C7 - 1023.

Hwang, H., Lee, K., Shin, M., Lee, G., & Lee, H. (2008). Flow characterization of valveless micropump using driving equivalent moment: Theory and experiments. Microfluidics and Nanofluidics 5:795-807.

Laser, J., & Santiago, G. (2004). A review of micropumps. Journal of Micromechanics and Microengineering 14:R35-R64.

Li, S., & Chen, S. (2003). Analytical analysis of a circular PZT actuator for valveless micropumps. Sensors and Actuators, A 104:151-161.

Lim, M., Lee, S., Park, C., Yoon, J., & Goo, S. (2005). Design and demonstration of a biomimetic wing section using a lightweight piezo-composite actuator (LIPCA). Smart Materials and Structures 14:496-503.

Ma, K., Hou, R., Lin, Y., & Gao, J. (2008). The improved performance of one-side actuating diaphragm micropump for a liquid cooling system. International Communications in Heat and Mass Transfer 35:957-966.

Olsson, A., Stemme, G., & Stemme, E. (1999). A numerical design study of the valveless diffuser pump using a lumped-mass model. Journal of Micromechanics and Microengineering 9:34-44.

Olsson, A., Stemme, G., & Stemme, E. (2000). Numerical and experimental studies of flat- walled diffuser elements for valve-less micropumps. Sensors and Actuators, A 84:165-175.

Singhal, V., & Garimella, V. (2005). A novel valveless micropump with electrohydrodynamic enhancement for high heat flux cooling. IEEE Transactions on Advanced Packaging 28:216-230.

Singhal V., Garimella V., & Murthy Y. (2004). Low Reynolds number flow through nozzle-diffuser elements in valveless micropumps. Sensors and Actuators, A 113:226-235.

Stemme, E., & Stemme, G. (1993). A valveless diffuser/nozzle-based fluid pump. Sensors and Actuators, A 39:159-167.

Tarik, B., & Jean-Paul, G. (1996). Modeling micropumps with electrical equivalent networks. Journal of Micromechanics and Microengineering 6:398-404.

Verma, P., Chatterjee, D., & Nagarajan, T. (2009). Design and development of a modular valveless micropump on a printed circuit board for integrated electronic cooling. Proceedings of the Institution of Mechanical Engineers, Part C: Journal of Mechanical Engineering Science 223:953-963.

Versteeg, K., & Malalasekera, W. (1995) An introduction to computational fluid dynamics: the finite volume method. Longman, Harlow.

Wang, B., Chu, X., Li, E., & Li, L. (2006). Simulations and analysis of a piezoelectric micropump. Ultrasonics 44:e643-e646.

Wu, T. (2003). Modeling and design of a novel cooling device for microelectronics using piezoelectric resonating beams. North Carolina State University, United States , North Carolina, pp. 224.

Yao, Q., Xu, D., Pan, L., Melissa, A., Ho, W., Lee, P., & Shabbir, M. (2007). CFD simulations of flows in valveless micropumps. Engineering Applications of Computational Fluid Mechanics 1:181-188.

Yi-Fang, H., Chen-Han, T., Chia-Jui, H., Yu-Ching, L., Takahito, O., & Yao-Chuan, T. (2020). Metallic glass thin film integrated with flexible membrane for electromagnetic micropump application. Japanese Journal of Applied Physics, vol. 59, no. SI, pp. SIIK03.

Zhang, L., & Wu, K. (2005). Numerical study of periodical flows of piezoelectric valveless micropump for biochips. Applied Mathematics and Mechanics (English Edition) 26:1026-1033.

Zhang, T., & Wang, M. (2006). Performance evaluation of a valveless micropump driven by a ring-type piezoelectric actuator. IEEE Transactions on Ultrasonics, Ferroelectrics, and Frequency Control 53:463-473.